AMERICAN SOCIETY FOR MICROBIOLOGY | Journal of Bacteriology®

RESEARCH ARTICLE

SwrD (YlzI) Promotes Swarming in *Bacillus subtilis* by Increasing Power to Flagellar Motors

Ashley N. Hall,[a] Sundharraman Subramanian,[b,c] Reid T. Oshiro,[a] Alexandra K. Canzoneri,[a] Daniel B. Kearns[a]

[a]Department of Biology, Indiana University, Bloomington, Indiana, USA
[b]Department of Molecular and Cellular Biochemistry, Indiana University, Bloomington, Indiana, USA
[c]Department of Chemistry, Indiana University, Bloomington, Indiana, USA

ABSTRACT The bacterium *Bacillus subtilis* is capable of two kinds of flagellum-mediated motility: swimming, which occurs in liquid, and swarming, which occurs on a surface. Swarming is distinct from swimming in that it requires secretion of a surfactant, an increase in flagellar density, and perhaps additional factors. Here we report a new gene, *swrD*, located within the 32 gene *fla-che* operon dedicated to flagellar biosynthesis and chemotaxis, which when mutated abolished swarming motility. SwrD was not required for surfactant production, flagellar gene expression, or an increase in flagellar number. Instead, SwrD was required to increase flagellar power. Mutation of *swrD* reduced swimming speed and torque of tethered flagella, and all *swrD*-related phenotypes were restored when the stator subunits MotA and MotB were overexpressed either by spontaneous suppressor mutations or by artificial induction. We conclude that swarming motility requires flagellar power in excess of that which is needed to swim.

IMPORTANCE Bacteria swim in liquid and swarm over surfaces by rotating flagella, but the difference between swimming and swarming is poorly understood. Here we report that SwrD of *Bacillus subtilis* is necessary for swarming because it increases flagellar torque and cells mutated for *swrD* swim with reduced speed. How flagellar motors generate power is primarily studied in *Escherichia coli*, and SwrD likely increases power in other organisms, like the *Firmicutes*, *Clostridia*, *Spirochaetes*, and the *Deltaproteobacteria*.

KEYWORDS flagella, motor, torque, swarming, *swrD*, *motA*, *motB*

Bacterial flagella drive two forms of active movement called swimming and swarming motility. During swimming motility, cells rotate helical flagella that act like propellers to push individuals through a three-dimensional liquid environment (1). Swarming motility also requires flagellar rotation, but swarming cells move as multicellular groups across a surface, within films of water approximately the depth of a single cell (2, 3). In the Gram-positive bacterium *Bacillus subtilis*, swarming is distinct from swimming in that it has additional physiological requirements, including the secretion of a surfactant and an increase in flagellar density on the surface of the cell (4, 5). The surfactant acts to reduce surface tension and create the thin layer of water within which to swarm. The reason that cells require an increase in flagellar density is unknown, but it may be necessary to increase the total amount of thrust generated by the cell.

Flagella rotate when consumption of the proton motive force powers a change in the interaction between the flagellar rotor and stator proteins. The rotor is a single gear-like structure (called the C-ring) made from many subunits of the proteins FliG, FliM, and FliN and sits on the cytoplasmic face of each membrane-anchored flagellum (6–9). The stators are complexes of membrane-bound proton channels made from two

Received 30 August 2017 **Accepted** 29 September 2017

Accepted manuscript posted online 23 October 2017

Citation Hall AN, Subramanian S, Oshiro RT, Canzoneri AK, Kearns DB. 2018. SwrD (YlzI) promotes swarming in *Bacillus subtilis* by increasing power to flagellar motors. J Bacteriol 200:e00529-17. https://doi.org/10.1128/JB.00529-17.

Editor George O'Toole, Geisel School of Medicine at Dartmouth

Address correspondence to Daniel B. Kearns, dbkearns@indiana.edu.

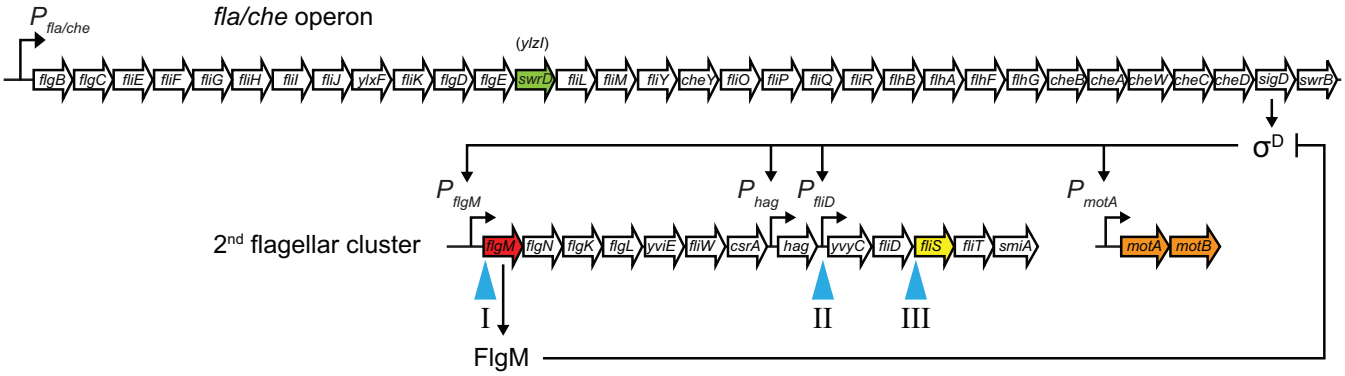

FIG 1 Genetic context of the *swrD* gene and suppressor of *swrD* (*sod*) mutations. The *swrD* gene (green arrow), formerly annotated as *ylzI*, is located within the *fla-che* operon (top row of arrows). Open arrows indicate open reading frames, bent arrows indicate promoters. Blue carets indicate the location of suppressor of *swrD* (*sod*) mutant classes in the second flagellar cluster containing σ^D-dependent genes unlinked to the *fla-che* operon. Red (*flgM*) and yellow (*fliS*) arrows indicate genes discussed further in the text. The diagram is not to scale.

subunits of MotB, which conducts protons, and four subunits of MotA, which interacts with the C-ring protein FliG (10, 11). When protons flow through MotB, a conformational change occurs in MotA that is thought to electrostatically push on FliG and create the torque for flagellar rotation (8, 10, 12–16). Stator number is dynamic, and torque is porportional to the number of stators associated with the flagellum (17–21). More torque-generating units are added commensurate with rotational load to create proportional power, and thus the flagellum operates as a constant torque motor (17, 22, 23). The biophysics of flagellar rotation has been studied primarily in *Escherichia coli* and *Salmonella enterica*, and while *B. subtilis* encodes similar motor proteins, its motor properties are less well understood.

Here we characterize *ylzI*, a gene of unknown function located within the large *fla-che* operon of flagellar and chemotaxis genes. We rename the *ylzI* gene and its gene product *swrD* and SwrD, respectively, as mutation of *swrD* abolished swarming but not swimming motility. The *swrD* mutant was not defective in surfactant production or involved in an increase in flagellar number, as found in other swarming mutants. Instead, the swarming defect was correlated with a decrease in swimming speed and a decrease in motor torque. Moreover, all phenotypes of the *swrD* mutant were bypassed by overexpression of MotA and MotB, suggesting that SwrD increased power via the flagellar stators. The *swrD* gene is coexpressed with the *motA* and *motB* genes in many organisms, including the spirochetes, which may require increased stator power to rotate their cell bodies in viscous environments.

RESULTS

SwrD is required for swarming motility. The gene *swrD* (*ylzI*) is located within the 32-gene, 27-kb *fla-che* operon and is predicted to encode SwrD, a 71-amino-acid protein of unknown function (Fig. 1). Cells mutated for SwrD are severely defective in swarming motility, a flagellum-dependent form of migration across a 0.7% agar surface (2, 24). To determine whether SwrD was required for swimming motility, in which flagella power movement through a loose agar matrix, cells were inoculated in the center of a 0.3% lysogeny broth (LB) agar plate and incubated for 12 h. Wild-type cells created a large zone of colonization by consuming nutrients locally and swimming up the resulting nutrient gradient by chemotaxis (Fig. 2) (25, 26). The zone of colonization was dramatically reduced when cells were mutated for either flagellar biosynthesis (*hag*) or chemotaxis (*cheA*) (Fig. 2). The *swrD* mutant exhibited a zone of colonization smaller than that of the wild-type cells, but the zone was larger than that made by the aflagellate and nonchemotactic mutants (Fig. 2). Finally, *swrD* mutant cells swam in liquid when observed via wet-mount phase-contrast microscopy. We conclude that SwrD is not strictly required for swimming motility.

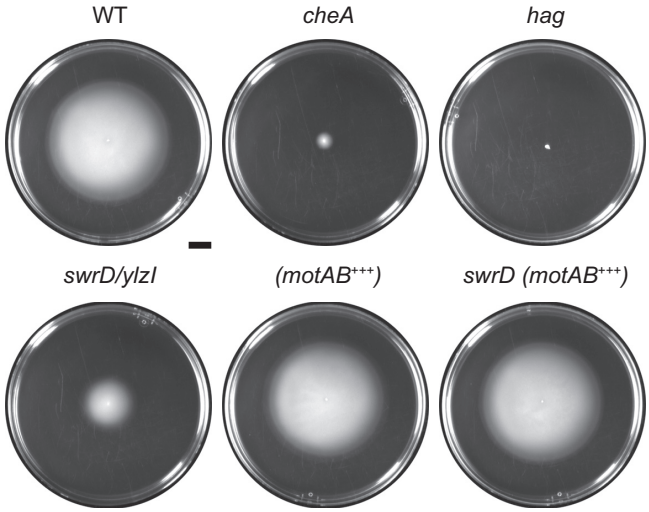

FIG 2 Cells mutated for *swrD* are modestly reduced for swimming motility. Circles are top views of 0.3% agar LB plates containing 1 mM IPTG, centrally inoculated with the indicated strain, grown for 12 h at 37°C, and filmed against a black background such that zones of colonization appear white and uncolonized agar appears black. In addition to the indicated background, each strain is also mutated for surfactin (to abolish swarming over the surface) and extracellular polysaccharide (to abolish sliding over the surface). The genotype is indicated above the corresponding plate. +++ indicates that the *motA* and *motB* genes were overexpressed by induction with 1 mM IPTG. The following strains were used to generate the figure: DK374 (wild type [WT]), DK2203 (*cheA*), DK378 (*hag*), DK1405 (*swrD*), DK5314 (*motAB*$^{+++}$), and DK5315 [*swrD* (*motAB*$^{+++}$)]. Scale bar, 1 cm.

The swarming defect of the *swrD* mutant could have been due to a polar effect on downstream genes, as *swrD* sits in the middle of the *fla-che* operon and the 3′ end of the *swrD* open reading frame overlaps with the 5′ end of the *fliL* gene located immediately downstream. To determine whether the absence of SwrD was responsible for the motility defect, a complementation construct was generated such that the *swrD* open reading frame was fused downstream of the native promoter of the *fla-che* operon, $P_{fla\text{-}che}$, and integrated at an ectopic locus (*amyE*::$P_{fla\text{-}che}$-*swrD*). The *swrD* mutant displayed a severe swarming defect, as previously reported, and a transparent watery ring surrounded the nonswarming colony, which indicated that surfactin was still being synthesized (4, 27) (Fig. 3A). When the *swrD* complementation construct was ectopically integrated in the *swrD* mutant, swarming motility was restored to wild-type levels (Fig. 3A). We conclude that the swarming defect of the *swrD* mutant is due to the absence of SwrD protein and not to polar effects on genes downstream in the *fla-che* operon. SwrD was named swarming motility protein D because it was required for swarming but not swimming, the swarming defect was not due to a lack of surfactant production, and it was the fourth protein with the Swr prefix in *B. subtilis* (28).

SwrD is not required for flagellar biosynthesis. One reason cells fail to swarm is because of the synthesis of an insufficient number of flagellar basal bodies, as found in cells mutated for the master activator of flagellar biosynthesis, SwrA (5, 29, 30). To determine whether the *swrD* mutant was defective in basal body synthesis, a *swrD* mutation was introduced into a strain in which the flagellar basal body could be detected as fluorescent puncta due to a fluorescent protein fused to the flagellar C-ring component protein FliM (31). Whereas cells mutated for *swrA* had a reduced number of FliM-green fluorescent protein (GFP) fluorescent puncta per cell, cells mutated for *swrD* had a number of puncta comparable to those of the wild-type swimming cells (Fig. 4A and B). Cells of the *swrD* mutant also had the capacity to increase flagellar basal body number, as basal body number increased when SwrA was overexpressed (Fig. 4B). Whereas overexpression of SwrA creates constitutively hyperflagellated cells (5, 31) and abolishes the swarming lag period in the wild type (29), SwrA overexpression did not restore swarming to the *swrD* mutant (Fig. 3B). We conclude that the *swrD* mutant has a defect in swarming motility unrelated to an increase in flagellar basal body number.

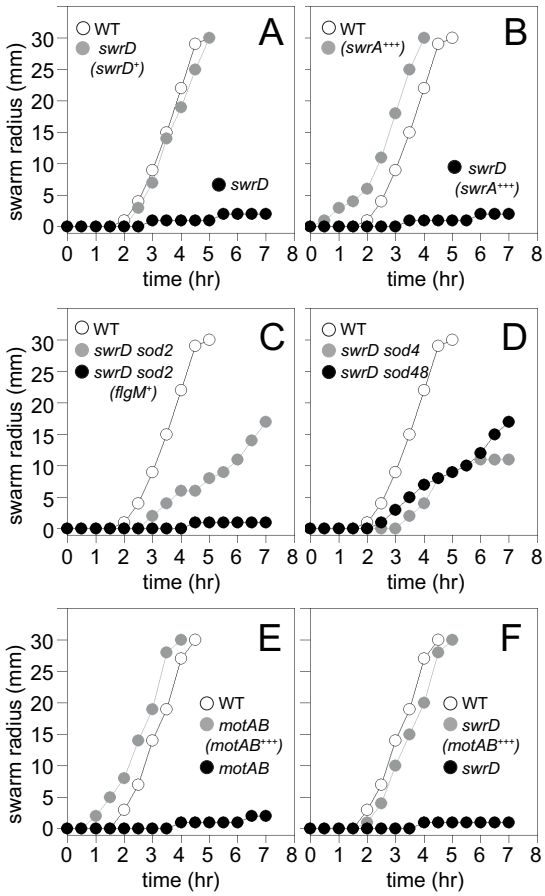

FIG 3 Cells mutated for *swrD* do not swarm, and swarming can be rescued by increasing the expression of *motAB*. (A to F) Quantitative swarm expansion assays. The relevant genotype of each strain is indicated within the graph. Gene names in parentheses indicate genes introduced at an ectopic locus. + indicates that genes are expressed from their native promoter. +++ indicates that the genes indicated have been overexpressed by the addition of 1 mM IPTG. Wild type (WT) data were reproduced in panels A to D and separately in panels E and F to match the experimental strains in the corresponding data set. Each data point is the average result of three replicates. The following strains were used to generate the data: in panel A, 3610 (WT), DS6657 (*swrD*), and DS7550 [*swrD* (*swrD*$^+$)]; in panel B, 3610 (WT), DK1597 [*swrD* (*swrA*$^{+++}$)], and DS860 (*swrA*); in panel C, 3610 (WT), DS6698 (*swrD sod2*), and DK1839 [*swrD sod2* (*flgM*$^+$)]; in panel D, 3610 (WT), DS7527 (*swrD sod4*), and DK48 (*swrD sod48*); in panel E, 3610 (WT), DS222 (*motAB*), and DK801 [*motAB* (*motAB*$^{+++}$)]; in panel F, 3610 (WT), DS6657 (*swrD*), and DK4651 [*swrD* (*motAB*$^{+++}$)].

Another reason cells fail to swarm is because of the synthesis of an insufficient number of flagellar hooks, as found in cells mutated for the activator of flagellar type III secretion, SwrB (32). To determine whether *swrD* mutants were defective in hook synthesis, a *swrD* mutant was introduced into a strain with an allele for the FlgE hook structural protein FlgE^{T123C} that could be fluorescently labeled by the addition of a fluorescent maleimide stain (33). Whereas cells mutated for SwrB had a reduced number of fluorescent hooks per cell, cells mutated for SwrD had a number of fluorescent hooks comparable to that of the wild type (Fig. 4C and D). Cells mutated for SwrD also had the capacity to increase the flagellar hook number, as hook number increased when SwrA was overexpressed (Fig. 4D), again despite being unable to restore swarming motility (Fig. 3B). We conclude that the *swrD* mutant has a defect in swarming motility unrelated to an increase in flagellar hook number.

Swarming motility likely requires an increase in the number of flagellar filaments, which depends on the activity of both SwrA (to increase basal bodies) and SwrB (to increase hooks). To determine whether the *swrD* mutant was specifically defective in flagellar filament synthesis, a *swrD* mutation was introduced into a strain with an allele

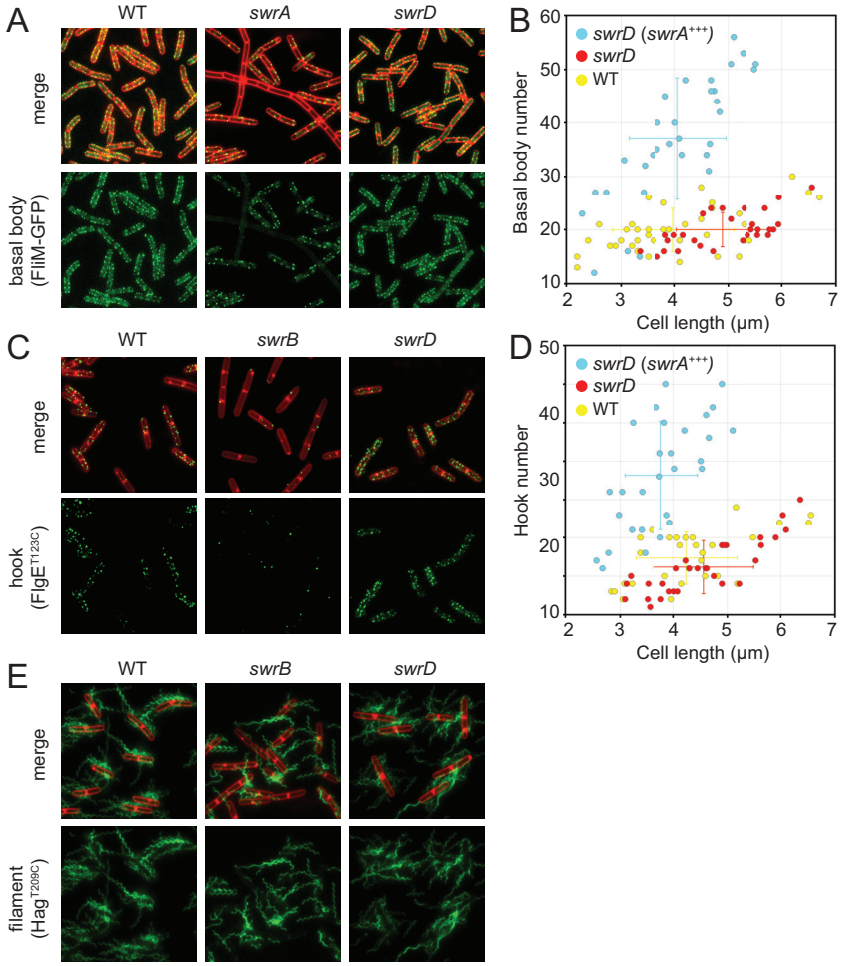

FIG 4 Cells mutated for *swrD* are not defective in flagellar assembly or flagellar number. (A) Fluorescence micrographs of wild-type (DS8521), *swrA* mutant (DS8600), and *swrD* mutant (DK1358) cells expressing the FliM-GFP fusion that indicates the location of flagellar basal bodies. (B) Three-dimensional structured illumination microscopy (3D SIM) was used to count the flagellar basal bodies (FliM-GFP puncta) per cell length in the wild type (DS8521), *swrD* mutant (DK1358), and *swrD swrA*$^{+++}$ mutant containing a $P_{hyspank}$-*swrA* construct grown in the presence of 1 mM IPTG (DK4616). (C) Fluorescence micrographs of wild-type (DS7673), *swrB* mutant (DK478), and *swrD* mutant (DK1359) cells expressing the FlgE^{T123C} allele that indicates the location of flagellar hooks when stained with a fluorescent maleimide dye. (D) 3D SIM was used to count the flagellar hooks (FlgE^{T123C} puncta) per cell length in the wild type (DS7673), *swrD* mutant (DK1359), and *swrD* mutant containing a $P_{hyspank}$-*swrA* construct (*swrA*$^{+++}$) grown in the presence of 1 mM IPTG (DK4724). (E) Fluorescence micrographs of wild-type (DS1916), *swrB* mutant (DS9319), and *swrD* mutant (DS8816) cells expressing the Hag^{T209C} allele that indicates the location of flagellar filaments when stained with a fluorescent maleimide dye.

for the Hag filament structural protein, Hag^{T209C}, that could be fluorescently labeled with a maleimide stain (34–36). Compared to the reduced number of flagella found in cells mutated for SwrB, cells mutated for SwrD appeared to have a number of fluorescent filaments qualitatively comparable to that of the wild type (Fig. 4E). With the caveat that we are currently unable to obtain an accurate count of the flagellar filaments per cell, *swrD* mutant cells do not appear to have a defect in flagellar assembly or flagellar number. We further conclude that cells mutated for SwrD are defective in swarming motility for reasons other than those found in cells mutated for either SwrA or SwrB. We infer that SwrD promotes an as-yet-unknown requirement for swarming motility in *B. subtilis*.

Enhanced σ^D activity restores swarming to cells that lack SwrD. To determine the mechanism by which SwrD activates swarming motility, spontaneous suppressors that restored swarming motility to a *swrD* mutant were isolated. Whereas a *swrD*

TABLE 1 Suppressor of *swrD* (*sod*) alleles[a]

Class and suppressor	Genotype	Strain
Class I (FlgM loss-of-function mutations)		
sod1	$flgM^{Q31\text{^}FS}$	DS6697
sod2	$flgM^{Q64*}$	DS6698
sod3	$flgM^{Q31\text{^}FS}$	DS6699
sod5	$flgM^{N17\text{^}FS}$	DS7528
sod6	$flgM^{V72*}$	DS7529
sod7	$flgM^{Q24*}$	DS7530
sod8	$flgM^{Q64*}$	DS8791
sod39	$flgM^{Q9*}$	DK39
sod40	$flgM^{Q64*}$	DK40
sod41	$flgM^{Q64*}$	DK41
sod42	$flgM^{Q64*}$	DK42
sod43	$flgM^{Q64*}$	DK43
sod44	$flgM^{T26\text{^}FS}$	DK44
sod46	$flgM^{N80\text{^}FS}$	DK46
sod47	$flgM^{Q64*}$	DK47
sod51	$flgM^{Q64*}$	DK615
sod52	$flgM^{Q64*}$	DK616
Class II (P_{fliD} promoter-down mutation): *sod4*	P_{fliD} **T**GTAAT→**C**GTAAT	DS7527
Class III (FliS translation-down mutation): *sod48*	$fliS^{RBS}$ **G**GAGG→**A**GAGG	DK48
Unidentified		
sod38	Unknown	DK38
sod50	Unknown	DK614

[a]Each *sod* mutation was independently isolated from a separate swarm plate, each inoculated with a separate colony of the DS6657 Δ*swrD* parent. Thus, although some of the mutations were identical, they are not siblings and represent independent genetic events. ^FS, frameshift after the indicated codon; *, stop codon. Bold letters indicate the nucleotide position changed by the mutation. Underlined letters indicate the −35 element of the P_{fliD} σ^D-dependent promoter. RBS, ribosome binding site or Shine-Dalgarno sequence.

mutant was severely defective for swarming motility and grew as a tight colony in the center of a swarm agar plate, upon prolonged incubation (~24 h), spontaneous mutations that restored swarming and emerged as flares of cells arose. In total, 21 suppressor of *swrD* (*sod*) mutants were independently isolated, and all but two were identified by classical transposon-assisted, SPP1-mediated generalized transduction genetic linkage mapping, followed by directed gene sequencing. All identified *sod* suppressor mutations genetically mapped to the second flagellar cluster of motility genes and, based on their genetic locations, were grouped into three different classes (Fig. 1; Table 1).

***sod* class I: FlgM loss-of-function mutations.** The *sod* class I suppressor mutations restored partial swarming to the *swrD* mutant (Fig. 3C). Linkage mapping and sequencing revealed that 17 out of 19 *sod* mutations (e.g., *sod2*) were either frameshift or nonsense truncations within the *flgM* gene, likely leading to FlgM loss of function (Fig. 1, *sod* class I). Consistent with a FlgM loss-of-function phenotype, introduction of an ectopically integrated complementation construct in which the wild-type *flgM* open reading frame was expressed under the control of its own promoter (*amyE*::P_{flgM}-*flgM*), restored a swarming defect to a *swrD sod* class I background (Fig. 3C). FlgM is the anti-sigma factor that inhibits σ^D-dependent gene expression (37–39). Consistent with loss of anti-sigma factor activity, expression increased from a series of β-galactosidase (*lacZ*) reporters fused to the σ^D-dependent promoters P_{hag}, P_{motA}, and P_{flgM} but not from the σ^A-dependent promoter $P_{fla\text{-}che}$ in the *swrD sod* class I mutant background (40–43) (Fig. 5A). We conclude that one way to restore swarming to a *swrD* mutant is to abolish FlgM and increase σ^D activity. We note, however, that mutation of *swrD* alone did not decrease the expression magnitude from the σ^D-dependent LacZ reporters nor did it decrease the expression frequency from a σ^D-dependent GFP reporter (Fig. 5A; see Fig. S1 in the supplemental material). We infer that SwrD does not act to

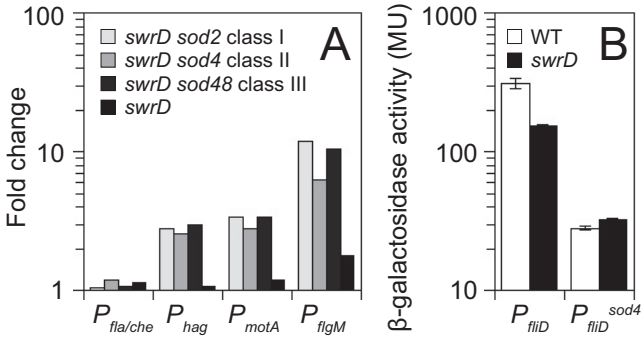

FIG 5 Suppressors of *swrD* (*sod*) increase σ^D-dependent gene expression. (A) Expression of various *lacZ* reporters fused to the promoter regions indicated along the *x* axis was measured in *swrD* and *swrD sod* mutant backgrounds. To generate each bar, the expression of each reporter in the various backgrounds was divided by the expression of the reporter in a wild-type background and expressed as a fold change. The raw data and strains used to generate this panel are presented in Table S3 in the supplemental material. (B) Expression of either P_{fliD} or P_{fliD}^{sod4} fused to *lacZ* in wild-type (WT) and *swrD* mutant backgrounds. Error bars are the standard deviation of results of three biological replicates.

generally increase σ^D activity and that the *sod* mutations that disrupt FlgM are likely compensatory rather than bypass suppressors.

***sod* class II: P_{fliD} promoter-down mutation.** The *sod* class II suppressor mutation *sod4* restored partial swarming to the *swrD* mutant (Fig. 3D). Linkage mapping and sequencing indicated that a single *sod* (*sod4*) was a mutation upstream of the P_{fliD} promoter (Fig. 1, *sod* class II). The mutation changed a T to a C 2 bp upstream of the −35 region of the σ^D-dependent promoter (**T**GTAAT to **C**GTAAT; −35 element sequence underlined) (44). To determine the consequence of the *sod* class II mutation, P_{fliD} reporters were generated by fusing either the wild type or the *sod4* mutant allele promoter region upstream of *lacZ*. Unlike other σ^D-dependent promoters, expression from P_{fliD} was reduced in the *swrD* mutant relative to the wild type, albeit only 2-fold (Fig. 5B). The swarming defect in a *swrD* mutant was not due to a specific reduction in P_{fliD} activity, however, as the *sod4* allele reduced expression from P_{fliD} another 10-fold relative to the wild type (Fig. 5B). We conclude that the P_{fliD}^{sod4} allele is a promoter-down mutation, and we infer that the 2-fold reduction of P_{fliD} activity in a *swrD* mutant may be a consequence, rather than a cause, of the *swrD* swarming motility defect. Finally, the s*wrD sod4* background showed an increase in the P_{hag}, P_{motA}, and P_{flgM} σ^D-dependent transcriptional reporters (Fig. 5A). Thus, the *sod* class II P_{fliD} promoter-down mutation restored swarming by increasing generalized σ^D activity like the *sod* class I mutations.

***sod* class III: FliS translation-down mutation.** The *sod* class III suppressor mutation (*sod48*) restored partial swarming to the *swrD* mutant (Fig. 3E). Linkage mapping and sequencing identified a mutation upstream of the *fliS* gene encoding the chaperone for flagellin secretion, FliS (45–47). The mutation was in the putative Shine-Dalgarno ribosome binding sequence, changing a G to an A (**G**GAGGA to **A**GAGGA) and moving it away from consensus (48). To determine the effect of the mutation on FliS expression, Western blot analysis was performed using anti-FliS as a primary antibody. FliS was present in the wild type and absent in a *fliS* deletion mutant. In the *swrD* null mutant, FliS levels appeared to be slightly higher than in the wild type (Fig. 6A). The *swrD sod48* mutation reduced FliS levels, supporting the idea that it had impaired the Shine-Dalgarno sequence and, thus, translation (Fig. 6A). FliS levels were not correlated with a rescue of swarming, however, as the *swrD sod4* (class II) and *swrD sod2* (class I) mutants showed reduced and elevated FliS levels relative to the *swrD* mutant, respectively (Fig. 6A). Finally, the s*wrD sod48* background showed an increase in the P_{hag}, P_{motA}, and P_{flgM} σ^D-dependent transcriptional reporters (Fig. 5A). We conclude that the restoration of swarming by the *sod* class III FliS translation-down mutation was not directly due to a reduced level of FliS but rather to an indirect increase in generalized σ^D activity.

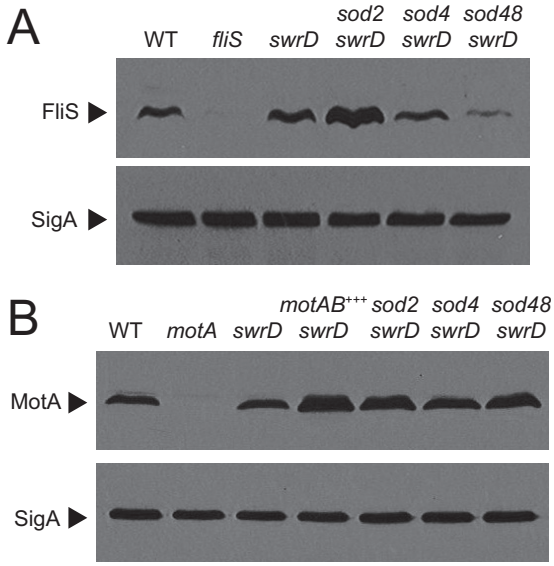

FIG 6 Rescue of swarming to a *swrD* mutant is correlated with elevated levels of MotA. (A) Western analysis of cell lysates resolved by SDS-PAGE and probed with anti-FliS and anti-SigA antibody (to serve as a loading control), respectively. The same samples were used to make each panel, but 10-fold less lysate was loaded in each lane for the anti-SigA Western blot. The following strains were used to generate the panel: 3610 (WT), DS7792 (*fliS*), DS6657 (*swrD*), DS6698 (*swrD sod2*), DS7527 (*swrD sod4*), and DK48 (*swrD sod48*). (B) Western analysis of cell lysates resolved by SDS-PAGE and probed with anti-MotA and anti-SigA antibody (to serve as a loading control), respectively. The same samples were used to make each panel, but 10-fold less lysate was loaded in each lane for the anti-SigA Western blot. The following strains were used to generate the panel: 3610 (WT), DS7498 (*motA* mutant), DS6657 (*swrD*), *swrD* $P_{hyspank}$-*motAB* mutant grown in the presence of 1 mM IPTG (*motAB*$^{+++}$) (DK4651), DS6698 (*swrD sod2*), DS7527 (*swrD sod4*), and DK48 (*swrD sod48*).

In summary, we conclude that all three *sod* suppressor classes were effectively similar in that they increased σ^D activity, albeit by different mechanisms. Class I mutations abolished activity of the anti-sigma factor FlgM directly, whereas class II and class III mutations reduced the synthesis of the flagellin secretion chaperone FliS at the transcriptional and translational levels, respectively. FlgM is antagonized by export through the flagellar secretion system, and reduced synthesis of FliS may reduce flagellin export, perhaps reducing substrate competition, thereby increasing FlgM secretion, and thus increasing free σ^D protein (24, 46, 47). Since there did not appear to be reduced expression from σ^D-dependent promoters in the *swrD* parental background, however, we infer that the *sod* suppressor mutants increase the expression of one or more σ^D-dependent genes that compensate for the lack of SwrD.

Cells lacking SwrD have a defect in flagellar power. There are many genes under the control of σ^D, and enhanced expression of one or more of them could compensate for the absence of SwrD (29, 49). We decided to focus our attention on the σ^D-dependent *motAB* operon, encoding the proton-conducting stator units MotA and MotB that power flagellar rotation, for the following reasons. First, colonies of a *swrD* mutant were mucoid in a manner dependent on PgsB, a protein required for the synthesis of secreted poly-γ-glutamate, and phenocopied colonies of cells mutated for *motA*, *motB*, or other genetic constructs that inhibited flagellar rotation (50, 51) (Fig. 7A). Second, in many bacteria, including *Clostridia*, *Spirochaetes*, and *Thermotogales*, genes encoding homologs of SwrD are located immediately upstream of the genes encoding MotA and MotB (Fig. 7B). Third, levels of the MotA protein appeared to be elevated in each of the *sod* suppressor classes in Western blot analysis (Fig. 6B). SwrD did not appear to be involved in regulating MotA levels, however, as MotA levels did not change in the *swrD* mutant. Thus, we hypothesized that the function of SwrD was related to flagellar stator activity in a way that could be bypassed by an excess of stators in the membrane.

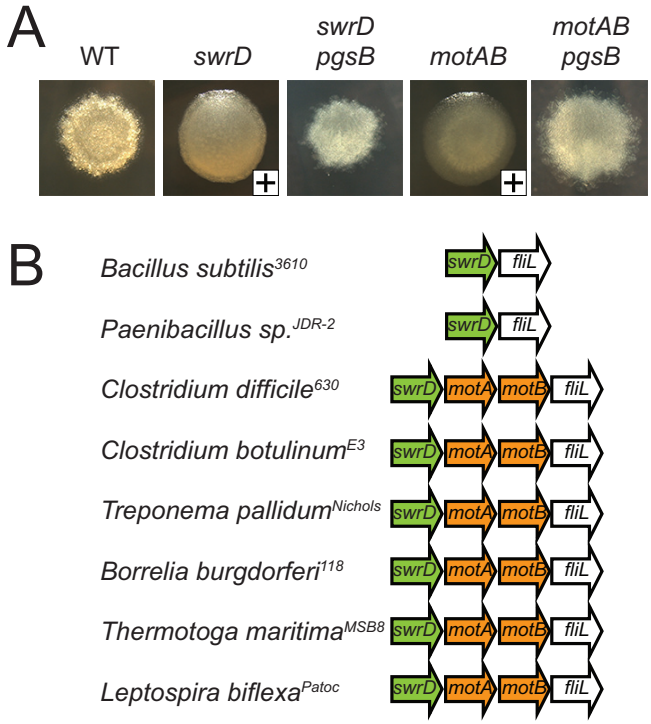

FIG 7 Colonies of a *swrD* mutant are mucoid. (A) Pictures of colonies of the indicated strain grown overnight at 37°C on a 1.5% LB agar plate. A plus sign in the lower right corner of the image indicates whether the colony was mucoid such that when touched with a toothpick, a sticky strand of poly-γ-glutamate was extracted. The following strains were used to generate this panel: 3610 (WT), DS6657 (*swrD*), DK3213 (*swrD pgsB*), DS222 (*motAB*), and DK3214 (*motAB pgsB*). (B) Cartoons of genetic neighborhoods with *swrD* homologs, as indicated at microbesonline.org. Arrows represent the indicated open reading frames, with *swrD* homologs colored green and *motA* or *motB* homologs colored orange.

To determine whether overexpression of *motA* and *motB* might be responsible for rescuing swarming motility to the *swrD* mutant in the various *sod* suppressors, both genes were cloned downstream of an IPTG (isopropyl-β-D-thiogalactopyranoside)-inducible $P_{hyspank}$ promoter and inserted at an ectopic site in the chromosome (*amyE*::$P_{hyspank}$-*motAB*). When the inducible construct was introduced into a *motAB* mutant, swarming motility was rescued in the presence but not the absence of 1 mM IPTG, indicating that the construct was expressed and capable of producing functional stators (Fig. 3E). When the inducible construct was introduced into a *swrD* mutant, both swarming motility and swimming motility were restored to wild-type levels in the presence of 1 mM IPTG and elevated levels of MotA were observed by Western blotting (Fig. 2, 3F, and 6B). We conclude that overexpression of flagellar stators is sufficient to compensate for the absence of SwrD and to rescue swarming motility. We infer that overexpression of *motA* and *motB* likely accounts for the swarming rescue of the various *sod* mutants.

We next wanted to determine whether the *swrD* mutant has a phenotype consistent with a defect in the flagellar stators. As MotA and MotB are also required for swimming motility, we monitored swimming speeds in various genetic backgrounds by phase-contrast microscopy and cell tracking software. Whereas wild-type cells swam with an average velocity of approximately 30 μm/s, *swrD* mutant cells swam 2-fold slower, with an average velocity of 15 μm/s (Fig. 8A). Overexpression of *motA* and *motB* increased the swimming speed of the *swrD* mutant to wild-type levels and did not increase the swimming speed further in the wild type (Fig. 8A). Swimming speed is the product of the approximately 17 flagella per cell (Fig. 4) (5). We next measured the effect of SwrD on individual flagella by observing cells rotating around a single tethered flagellum and calculating flagellar torque. Flagella of the *swrD* mutant generated 6-fold-less torque

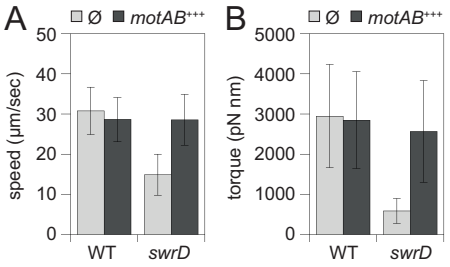

FIG 8 Cells mutated for SwrD have reduced swimming speed and flagellar torque. (A) Swim speed analysis of wild-type (DK4987) and *swrD* mutant (DK5022) cells unmodified (gray bars) or wild-type (DK5029) and *swrD* mutant (DK5030) cells in which the *motA* and *motB* genes were overexpressed by induction with 1 mM IPTG (black bars). Swimming velocity was calculated for 100 cells, and the average and standard deviation are reported. (B) Torque values of singly tethered wild-type (DK4987) and *swrD* mutant (DK5022) cells (gray bars) or wild-type (DK5029) and *swrD* mutant (DK5030) cells in which the *motA* and *motB* genes were overexpressed by induction with 1 mM IPTG (black bars). Torque values were calculated for 40 cells tethered by a single flagellum.

than the wild type, and wild-type torque values were restored to the *swrD* mutant when *motA* and *motB* were overexpressed (Fig. 8B). We conclude that SwrD is required for swarming because it is required to increase flagellar power in a manner that can be compensated for by extra copies of MotA and MotB in the membrane.

DISCUSSION

Swarming motility is a flagellum-mediated form of surface movement, and in *B. subtilis*, swarming requires an increase in flagellar density above a strict threshold (5). Motile, liquid-grown cells introduced to a surface experience a lag of approximately 1 to 2 h prior to swarming, during which the flagellar density on the cell surface doubles (5). At least two regulators are required for the surface-dependent increase in flagellar number: SwrA activates transcription of the *fla-che* operon to increase the number of flagellar basal bodies (29, 31), and SwrB activates flagellar type III secretion to increase the number of flagellar hooks (32). Precisely why an increase in flagellar density is required to swarm is unknown, but each additional flagellum adds to the total thrust of the cell, and perhaps a threshold amount of power is necessary to overcome surface forces. Here we report and characterize another protein required for swarming, SwrD, that is not impaired for flagellar number but is impaired in the torque generated by each flagellum.

SwrD is a 71-amino-acid protein encoded within the *B. subtilis fla-che* operon, and mutation of SwrD results in a 6-fold reduction in flagellar torque that may be overcome by specifically overexpressing the flagellar stator components MotA and MotB. The mechanism by which SwrD increases torque is unknown save that MotA protein levels were not impaired in a *swrD* mutant and thus SwrD appears to act at the level of MotAB activity. The MotAB stator complexes in *E. coli* dynamically associate with the basal body, where torque increases and decreases with stator association and dissociation (17, 18). If stators are also dynamic in *B. subtilis* in the absence of SwrD, then MotAB overexpression may increase the probability or duration (duty ratio) of stator-rotor interaction (52, 53). Thus, SwrD could be a tether that retains MotAB at the basal bodies to decrease stator dynamism and increase stator association in the wild type. Perhaps consistent with stator association, SwrD activity appears related to stator-rotor stoichiometry, as the *swrD* phenotype was overcome by increasing stators relative to rotors but was not overcome by increasing expression of all flagellar genes at the same ratio (e.g., SwrA overexpression). Although results with overexpression of MotA and MotB point to stator dynamism, we have not been able to generate a functional fluorescent fusion to either protein in *B. subtilis*, and thus stator dynamism is not directly testable. Whether SwrD interacts with MotAB, whether it interacts with other basal body components, or whether it functions intracellularly or extracellularly is currently unknown.

In *B. subtilis*, the gene encoding SwrD is located immediately upstream of, and may be translationally coupled with, the gene that encodes FliL. Primarily studied in *Proteobacteria* that lack SwrD, FliL associates with the basal body and deletion of FliL reduces swimming speed and motor torque (54–58). Further, FliL has been implicated in the regulation of swarming motility in both *Proteus mirabilis* and *Salmonella enterica* (57, 59–61). In *B. subtilis*, however, disruption of FliL results in a swarming motility defect that is less severe than that caused by disruption of SwrD, and unlike cells mutated for *swrD*, cells mutated for *fliL* did not experience improved swarming when MotA and MotB were overexpressed (see Fig. S2 in the supplemental material). Thus, while FliL and SwrD both increase flagellar power, we infer that they may do so by different mechanisms.

In summary, we conclude that a net increase in flagellar thrust is needed for *B. subtilis* to swarm. One way to increase power is to increase the flagellar density, controlled, at least in part, by SwrA and SwrB. Another way to increase total power is to increase the torque of each flagellum, controlled, at least in part, by SwrD. Neither strategy is sufficient to swarm, however, and both flagellar number and flagellar torque must be increased. Whereas SwrA and SwrB are narrowly conserved, phylogenetic analysis suggests that SwrD is found in a broad distribution of bacteria and is often encoded upstream of MotA and MotB (Fig. S3). We note that one phylum of bacteria that encodes SwrD is the *Spirochaetes*. Pathogenic spirochetes navigate viscous environments and can move between tight junctions of eukaryotic cells during infections, two behaviors that may require increased flagellar power. We suspect that SwrD may also increase torque to spirochete endoflagella and may be required for virulence.

MATERIALS AND METHODS

Strains and growth conditions. *B. subtilis* strains were grown in lysogeny broth (LB) (10 g tryptone, 5 g yeast extract, 5 g NaCl [per liter]) broth or on LB plates fortified with 1.5% Bacto agar at 37°C. When appropriate, antibiotics were included at the following concentrations: 10 μg/ml tetracycline, 100 μg/ml spectinomycin, 5 μg/ml chloramphenicol, 5 μg/ml kanamycin, and 1 μg/ml erythromycin plus 25 μg/ml lincomycin (*mls*). Isopropyl-β-D-thiogalactopyranoside (IPTG; Sigma) was added to the medium at the indicated concentration when appropriate.

Swarm expansion assay. Cells were grown to mid-log phase at 37°C in LB broth and resuspended to an optical density at 600 nm (OD_{600}) of 10 in pH 8.0 phosphate-buffered saline (PBS) buffer (137 mM NaCl, 2.7 mM KCl, 10 mM Na_2HPO_4, and 2 mM KH_2PO_4) containing 0.5% India ink (Higgins). Freshly prepared LB containing 0.7% Bacto agar (25 ml/plate) was dried for 10 min in a laminar flow hood, centrally inoculated with 10 μl of the cell suspension, dried for another 10 min, and incubated at 37°C (4). The India ink demarks the origin of the colony, and the swarm radius was measured relative to the origin. For consistency, an axis was drawn on the back of the plate and swarm radius measurements were taken along this transect. For experiments including IPTG, cells were propagated in broth in the presence of IPTG, and IPTG was included in the swarm agar plates. All experiments containing IPTG in this study were performed with a concentration of 1 mM IPTG.

Swim motility assay. For swim videos, cells were grown to mid-log phase (~0.6 OD_{600}) and a hanging drop wet mount was prepared. Video was captured with a Nikon 80i microscope with a Nikon Plan Apo 100× phase-contrast objective using MetaMorph software. For swim plate assays, cells were toothpick inoculated into LB containing 0.3% Bacto agar (25 ml/plate).

Strain construction. All PCR products were amplified from *B. subtilis* genomic DNA from the indicated strains. Constructs built were either introduced into the domesticated *B. subtilis* strain PY79 or the ancestral, competent cured plasmid strain DS2569 and transferred to the 3610 background via SPP1-mediated phage transduction or transformed directly into DK1042 (3610 *comI*^{Q12L}) (62). All strains used in this study are listed in Table 2. All primers used to build strains for this study are listed in Table S1 in the supplemental material, and all plasmids are listed in Table S2 in the supplemental material.

Complementation construct. To generate the *amyE*::$P_{fla\text{-}che}$-*swrD cat* ectopic *swrD* complementation construct, a PCR product containing *swrD* was amplified from chromosomal 3610 DNA with primer pair 2462/2463 and digested with BamHI and XhoI, and the $P_{fla\text{-}che}$ promoter was amplified from 3610 DNA with primer pair 1802/2460 and digested with XhoI and EcoRI. The fragments were simultaneously ligated into the BamHI and EcoRI sites of pDG364, which carries a chloramphenicol resistance marker and a polylinker between two arms of the *amyE* gene, to generate pDP329 (63).

LacZ reporter fusions. The P_{fliD} region was amplified separately from 3610 and DS7527 chromosomal DNA with primer pair 609/1510 and digested with HindIII and EcoRI. The fragment was ligated into the HindIII and EcoRI sites of pDG268, which carries a chloramphenicol resistance marker and a polylinker upstream of the *lacZ* gene between two arms of the *amyE* gene, to create pANR21 and pANR22, respectively (64).

SPP1 phage transduction. Serial dilutions of SPP1 phage stock were added to 0.2 ml of dense *B. subtilis* culture grown in TY broth (LB supplemented with 10 mM $MgSO_4$ and 100 μM $MnSO_4$, added after

TABLE 2 *Bacillus subtilis* strains

Strain	Genotype (reference)
3610	Wild type
DK38	Δ*swrD sod38*
DK39	Δ*swrD sod39* (*flgM*^{Q9*})
DK40	Δ*swrD sod40* (*flgM*^{Q64*})
DK41	Δ*swrD sod41* (*flgM*^{Q64*})
DK42	Δ*swrD sod42* (*flgM*^{Q64*})
DK43	Δ*swrD sod43* (*flgM*^{Q64*})
DK44	Δ*swrD sod44* (*flgM*$^{T26\wedge FS}$)
DK46	Δ*swrD sod46* (*flgM*$^{N80\wedge FS}$)
DK47	Δ*swrD sod47* (*flgM*^{Q64*})
DK48	Δ*swrD sod48* (*fliS*^{RBS} **G**GAGG→**A**GAGG)
DK67	Δ*swrD amyE*::$P_{fla\text{-}che}$-*lacZ cat*
DK68	Δ*swrD amyE*::P_{hag}-*lacZ cat*
DK374	*srfAC*::Tn*10 spec epsH*::*tet* (45)
DK378	Δ*hag srfAC*::Tn*10 spec epsH*::*tet* (45)
DK478	*swrB*::*tet* Δ*flgE amyE*::$P_{fla\text{-}che}$-*flgE*^{T123C} *cat* (32)
DK614	Δ*swrD sod50*
DK615	Δ*swrD sod51* (*flgM*^{Q64*})
DK616	Δ*swrD sod52* (*flgM*^{Q64*})
DK801	*motAB*::*tet amyE*::$P_{hyspank}$-*motAB spec*
DK1042	*comI*^{Q12L} (62)
DK1358	Δ*swrD* Δ*fliM amyE*::$P_{fla\text{-}che}$-*fliM-GFP spec*
DK1359	Δ*swrD* Δ*flgE amyE*::$P_{fla\text{-}che}$-*flgE*^{T123C} *cat*
DK1405	Δ*swrD srfAC*::*Tn10 spec epsH*::*tet*
DK1597	Δ*swrD amyE*::$P_{hyspank}$-*swrA spec*
DK1839	Δ*swrD sod2 amyE*::P_{flgM}-*flgM cat*
DK2203	Δ*cheA srfAC*::*Tn10 spec epsH*::*tet*
DK2907	Δ*swrD sod48 amyE*::P_{motA}-*lacZ cat*
DK2919	Δ*swrD sod4 amyE*::P_{motA}-*lacZ cat*
DK2925	Δ*swrD amyE*::P_{flgM}-*lacZ cat*
DK2926	Δ*swrD sod2 amyE*::P_{flgM}-*lacZ cat*
DK2927	Δ*swrD sod4 amyE*::P_{flgM}-*lacZ cat*
DK2929	Δ*swrD sod48 amyE*::P_{flgM}-*lacZ cat*
DK2968	Δ*swrD sod4 amyE*::P_{hag}-*lacZ cat*
DK2970	Δ*swrD sod48 amyE*::P_{hag}-*lacZ cat*
DK3046	Δ*swrD amyE*::P_{motA}-*lacZ cat*
DK3187	Δ*swrD sod4 amyE*::$P_{fla\text{-}che}$-*lacZ cat*
DK3188	Δ*swrD sod48 amyE*::$P_{fla\text{-}che}$-*lacZ cat*
DK3213	Δ*swrD pgsB*::*Tn10 spec*
DK3214	*motAB*::*tet pgsB*::*Tn10 spec*
DK4616	Δ*swrD* Δ*fliM amyE*::$P_{fla\text{-}che}$-*fliM-GFP spec thrC*::$P_{hyspank}$-*swrA mls*
DK4651	Δ*swrD amyE*::$P_{hyspank}$-*motAB spec*
DK4724	Δ*swrD* Δ*flgE amyE*::$P_{fla\text{-}che}$-*flgE*^{T123C} *cat thrC*::$P_{hyspank}$-*swrA mls*
DK4757	Δ*swrD sod2 amyE*::P_{hag}-*lacZ cat*
DK4758	Δ*swrD sod2 amyE*::$P_{fla\text{-}che}$-*lacZ cat*
DK4759	Δ*swrD sod2 amyE*::P_{motA}-*lacZ cat*
DK4987	Δ*cheB comI*^{Q12L}
DK4698	*amyE*::P_{fliD}-*lacZ cat*
DK4699	Δ*swrD amyE*::P_{fliD}-*lacZ cat*
DK4805	*amyE*::P_{fliD}^{sod4}-*lacZ cat*
DK4812	Δ*swrD amyE*::P_{fliD}^{sod4}-*lacZ cat*
DK5022	Δ*swrD* Δ*cheB comI*^{Q12L}
DK5029	Δ*swrD* Δ*cheB amyE*::$P_{hyspank}$-*motAB spec comI*^{Q12L}
DK5030	Δ*cheB amyE*::$P_{hyspank}$-*motAB spec comI*^{Q12L}
DK5113	Δ*fliL amyE*::$P_{hyspank}$-*motAB spec*
DK5314	*epsH*::*tet srfAA*::*mls amyE*::$P_{hyspank}$-*motAB spec*
DS5315	Δ*swrD epsH*::*tet srfAA*::*mls amyE*::$P_{hyspank}$-*motAB spec*
DS222	*motAB*::*tet* (51)
DS791	*amyE*::$P_{fla\text{-}che}$-*lacZ cat* (29)
DS793	*amyE*::P_{hag}-*lacZ cat* (29)
DS811	*amyE*::$_{flgM}$-*lacZ cat* (29)
DS860	*amyE*::$P_{hyspank}$-*swrA spec* (29)
DS908	*amyE*::P_{hag}-*GFP cat* (29)
DS1849	*amyE*::P_{motA}-*lacZ cat* (43)
DS1916	*amyE*::P_{hag}-*hag*^{T209C} *spec* (36)
DS6540	Δ*fliL* (24)

(Continued on next page)

TABLE 2 (Continued)

Strain	Genotype (reference)
DS6657	Δ*swrD* (24)
DS6697	Δ*swrD sod1* (*flgM*$^{Q31\wedge FS}$)
DS6698	Δ*swrD sod2* (*flgM*^{Q64*})
DS6699	Δ*swrD sod3* (*flgM*$^{Q31\wedge FS}$)
DS7498	Δ*motA* (51)
DS7527	Δ*swrD sod4* (P_{fliD} **T**GTAAT→**C**GTAAT)
DS7528	Δ*swrD sod5* (*flgM*$^{N17\wedge FS}$)
DS7529	Δ*swrD sod6* (*flgM*^{V72*})
DS7530	Δ*swrD sod7* (*flgM*^{Q64*})
DS7550	Δ*swrD amyE*::$P_{fla\text{-}che}$-*swrD cat*
DS7673	Δ*flgE amyE*::$P_{fla\text{-}che}$-*flgE*^{T123C} *cat* (33)
DS7696	Δ*fliL amyE*::P_{hag}-*GFP cat* (24)
DS7792	Δ*fliS* (45)
DS8521	Δ*fliM amyE*::$P_{fla\text{-}che}$-*fliM-GFP spec* (31)
DS8600	Δ*swrA* Δ*fliM amyE*::$P_{fla\text{-}che}$-*fliM-GFP spec* (31)
DS8791	Δ*swrD sod8* (*flgM*^{Q64*})
DS8816	Δ*swrD amyE*::P_{hag}-*hag*^{T209C} *spec*
DS9319	Δ*swrB amyE*::P_{hag}-*hag*^{T209C} *spec*
PY79	*sfp*^{0} *swrA*

autoclaving), and the mixture was incubated statically at 37°C for 15 min. Three milliliters of TYSA (molten TY broth supplemented with 0.5% agar) was added to each mixture and poured onto fresh TY plates, and the mixture was incubated at 30°C overnight. The top agar from the plate containing clear phage plaques was harvested by scraping it into a 15-ml conical tube, vortexing it, and centrifuging it at 6,500 × *g* for 10 min. The lysate was treated with 25 μg/ml DNase before being passed through a 0.45-μm syringe and being stored at 4°C.

Recipient cells were grown to stationary phase in 3 ml TY broth at 37°C. Cells (1 ml) were mixed with 9 ml of TY and 15 μl donor SPP1 phage stock (chloramphenicol, kanamycin, and spectinomycin markers) or 5 μl donor SPP1 phage stock (*mls* and tetracycline reporters). The mixture was incubated at room temperature with gentle rocking for 30 min. The transduction mixture was centrifuged at 6,500 × *g* for 5 min, the supernatant was discarded, and the pellet was resuspended in the remaining volume. One hundred microliters of the suspension was plated on LB medium fortified with 1.5% agar and the appropriate antibiotic (65).

Microscopy. Fluorescence microscopy was performed with a Nikon 80i microscope with a Nikon Plan Apo 100× phase-contrast objective and an Excite 120 metal halide lamp. FM 4-64 dye was visualized with a C-FL HYQ Texas Red filter cube (excitation filter, 532 to 587 nm; barrier filter, >590 nm). GFP was visualized using a C-FL HYQ fluorescein isothiocyanate (FITC) filter cube (FITC, excitation filter, 460 to 500 nm; barrier filter, 515 to 550 nm). Images were captured with a Photometrics Coolsnap HQ2 camera in black and white, false colored, and superimposed using MetaMorph image software. Counting of flagellar basal bodies and hooks was performed on an OMX three-dimensional structured illumination microscope (3D SIM) in the Light Microscopy Imaging Center (LMIC), Indiana University, and quantification was performed using the Imaris image analysis software.

For GFP microscopy, cells were grown in LB medium to an OD_{600} of 0.6 to 1.0. One milliliter was harvested, resuspended in 50 μl of 1× PBS buffer (137 mM NaCl, 2.7 mM KCl, 10 mM Na_2HPO_4, and 2 mM KH_2PO_4) containing 5 μg/ml FM 4-64, incubated for 3 min at room temperature, pelleted, washed two times with 1 ml of 1× PBS buffer, and finally resuspended to an OD_{600} of 10 in 1× PBS. A 4.5-μl suspension volume was spotted on a glass slide and immobilized with a poly-L-lysine-treated glass coverslip prior to microscopy.

For fluorescence microscopy of flagella and flagellar hooks, 1 ml of broth culture was harvested at an OD_{600} of 0.5 to 1.0 and washed once in 1.0 ml of 1× PBS buffer (137 mM NaCl, 2.7 mM KCl, 10 mM Na_2HPO_4, and 2 mM KH_2PO_4). The suspension was pelleted, resuspended in 50 μl of PBS buffer containing 5 μg/ml Alexa Fluor 488 C_5 maleimide (Molecular Probes), and incubated for 5 min at room temperature. Cells were then washed once with 1 ml PBS buffer. When appropriate, membranes were stained by resuspension in 50 μl of PBS buffer containing 5 μg/ml FM 4-64 (Molecular Probes) and incubated for 10 min at room temperature. Three microliters of suspension was placed on a microscope slide and immobilized with a poly-L-lysine-treated coverslip.

Western blotting. Strains were grown to mid-log phase, concentrated to an OD_{600} of 10 in lysis buffer (17.2 mM Tris [pH 7.0], 8.6 mM EDTA [pH 8.0], 1 mg/ml lysozyme, 0.1 mg/ml RNase A, 20 μg/ml DNase I, and 50 μg/ml phenylmethane sulfonyl fluoride) and incubated at 37°C for 30 min. SDS sample buffer (500 mM Tris [pH 6.8], 22% glycerol, 10% SDS, and 0.12% bromophenol blue) was added, and samples were boiled for 5 min. Twelve-microliter volumes of boiled samples were loaded onto 10% polyacrylamide native (with no added SDS) or 15% polyacrylamide denaturing (with 0.1% SDS) gels. Lysates were resolved at 150 V for 1.25 h, transferred onto nitrocellulose membranes, and subsequently probed with a 1:10,000 dilution of anti-FliS, a 1:3,000 dilution of anti-MotA (66), or a 1:80,000 dilution of anti-SigA polyclonal antiserum. Following incubation with the primary antibodies, nitrocellulose membranes were probed with horseradish peroxidase-conjugated goat anti-rabbit immunoglobulin G. Blots were developed using Pierce ECL substrate (Thermo Fisher Scientific).

FliS antibody preparation. One milligram of purified FliS protein (45) was sent to Cocalico Biologicals for serial injection into a rabbit host for antibody generation. Anti-FliS serum was mixed with FliS-conjugated Affigel-10 beads and incubated overnight at 4°C. Beads were packed onto a 1-cm column (Bio-Rad) and then washed with 100 mM glycine (pH 25) to release the antibody and immediately neutralized with 2 M Tris base. Purification of the antibody was verified by SDS-PAGE. Purified anti-FliS antibody was dialyzed into 1× PBS (pH 7.4) supplemented with 50% glycerol and stored at −80°C.

Swimming velocity analysis. Cells were grown to an OD_{600} of ~0.6 and then resuspended to an OD_{600} of 0.2 in LB medium. Tunnel slides were prepared by placing two coverslips with an ~2-cm gap in between them on a glass slide, and a third coverslip was placed over them; all the coverslips were secured using nail polish strengthener. The cells were then introduced into the tunnel slides and imaged using a Nikon 80i microscope with a Nikon Plan Apo 40× phase-contrast objective, and videos were recorded using a Photometrics Coolsnap HQ2 camera in black and white for 30 s at 5 frames per second. The videos were then analyzed by MicrobeJ (67) tracking software, and the velocity was determined using the MOTION.Velocity function (100 cells for each strain).

Torque calculation. Cells were grown to an OD_{600} of ~0.6 and then resuspended to an OD_{600} of 0.2 in LB medium. The cells were then introduced into the tunnel slides (see "Swimming velocity analysis"), singly tethered cells were then monitored using a Nikon 80i microscope with a Nikon Plan Apo 40× phase-contrast objective, and videos were recorded using a Photometrics Coolsnap HQ2 camera in black and white for 90 s at 3 fps. The angle traveled by the cells in radians as a function of time was calculated by utilizing the theta.ORIENTATION function (40 cells for each strain) in MicrobeJ (67). Torque is calculated using the formula $N_r = (C_r + r^2C_t)2\pi f$, where r is the distance between the center of rotation and the center of mass of a cell, f is the rotation rate, and C_r and C_t are rotational and translational frictional drag coefficients, respectively (68). With the cell approximated as a prolate ellipsoid, $C_r = (8\pi\eta a^3/3)/(\ln 2a/b - 0.5)$ and $C_t = 8\pi\eta a/(\ln 2a/b + 0.5)$, where a is cell length divided by 2 and b is cell width divided by 2.

***β*-Galactosidase assay.** Cells were grown to an OD_{600} of ~0.7 to 1.3 in LB medium in triplicate. One milliliter of each sample was harvested and resuspended in 1 ml of Z buffer (40 mM HaH_2PO_4, 60 mM Na_2HPO_4, 1 mM $MgSO_4$, 10 mM KCl, and 38 mM β-mercaptoethanol). Lysozyme was added to each sample to a final concentration of 0.2 mg/ml, and samples were incubated for 15 min at 30°C and thereafter kept on ice. Each sample was diluted appropriately to a final volume of 500 μl in Z buffer, and the reaction was started with 100 μl of 4 mg/ml *o*-nitrophenyl-β-D-galactopyranoside (in Z buffer) and stopped with 250 μl of 1 M Na_2CO_3. The OD_{420} of the reaction mixtures was recorded, and the β-galactosidase activity was calculated with the following formula [OD_{420}/(time in minutes × OD_{600})] × dilution factor × 1,000. All reactions were stopped prior to saturation of yellow color ($A_{420} < 1.2$). For those reactions with low to no β-galactosidase activity, the reaction was run for a maximum of 1 h before stopping.

SUPPLEMENTAL MATERIAL

Supplemental material for this article may be found at https://doi.org/10.1128/JB.00529-17.

SUPPLEMENTAL FILE 1, PDF file, 0.3 MB.

SUPPLEMENTAL FILE 2, XLSX file, 0.1 MB.

ACKNOWLEDGMENTS

We thank Rebecca Calvo, Jia-Mun Chan, Tim Chu, Adrien Ducret, and Patrick Eichenberger for intellectual and technical support. We thank Katherine Hummels for generation of the *swrD* phylogenetic tree. We thank Masahiro Ito for the anti-MotA antibody.

National Institutes of Health grant GM093030 to D.B.K. supported the work.

REFERENCES

1. Berg HC. 2003. The rotary motor of bacterial flagella. Annu Rev Biochem 72:19–54. https://doi.org/10.1146/annurev.biochem.72.121801.161737.
2. Kearns DB. 2010. A field guide to bacterial swarming motility. Nat Rev Microbiol 8:634–644. https://doi.org/10.1038/nrmicro2405.
3. Wu Y, Berg HC. 2012. Water reservoir maintained by cell growth fuels the spreading of a bacterial swarm. Proc Natl Acad Sci U S A 109:4128–4133. https://doi.org/10.1073/pnas.1118238109.
4. Kearns DB, Losick R. 2003. Swarming motility in undomesticated *Bacillus subtilis*. Mol Microbiol 49:581–590. https://doi.org/10.1046/j.1365-2958.2003.03584.x.
5. Mukherjee S, Bree AC, Liu J, Patrick JE, Chien P, Kearns DB. 2015. Adaptor-mediated Lon proteolysis restricts *Bacillus subtilis* hyperflagellation. Proc Natl Acad Sci U S A 112:250–255. https://doi.org/10.1073/pnas.1417419112.
6. Garza AG, Harris-Haller LW, Stoebner RA, Manson MD. 1995. Motility protein interactions in the bacterial flagellar motor. Proc Natl Acad Sci U S A 92:1970–1974. https://doi.org/10.1073/pnas.92.6.1970.
7. Marykwas DL, Schmidt SA, Berg HC. 1996. Interacting components of the flagellar motor of *Escherichia coli* revealed by the two-hybrid system in yeast. J Mol Biol 256:564–576. https://doi.org/10.1006/jmbi.1996.0109.
8. Tang H, Braun TF, Blair DF. 1996. Motility protein complexes in the bacterial flagellar motor. J Mol Biol 261:209–221. https://doi.org/10.1006/jmbi.1996.0453.
9. Thomas DR, Francis NR, Xu C, DeRosier DJ. 2006. The three-dimensional structure of the flagellar rotor from a clockwise-locked mutant of *Salmonella enterica* serovar Typhimurium. J Bacteriol 188:7039–7048. https://doi.org/10.1128/JB.00552-06.
10. Zhou J, Lloyd SA, Blair DF. 1998. Electrostatic interactions between rotor and stator in the bacterial flagellar motor. Proc Natl Acad Sci U S A 95:6436–6441. https://doi.org/10.1073/pnas.95.11.6436.

11. Kojima S, Blair DF. 2004. Solubilization and purification of the MotA/MotB complex of *Escherichia coli*. Biochemistry 43:26–34. https://doi.org/10.1021/bi035405l.
12. Khan S, Macnab RM. 1980. Proton chemical potential, proton electrical potential and bacterial motility. J Mol Biol 138:599–614. https://doi.org/10.1016/S0022-2836(80)80019-2.
13. Shioi J-I, Matsuura S, Imae Y. 1980. Quantitative measurements of proton motive force and motility in *Bacillus subtilis*. J Bacteriol 144:891–897.
14. Zhou J, Sharp LL, Tang HL, Lloyd SA, Billings S, Braun TF, Blair DF. 1998. Function of protonatable residues in the flagellar motor of *Escherichia coli*: a critical role for Asp 32 of MotB. J Bacteriol 180:2729–2735.
15. Kojima S, Blair DF. 2001. Conformational change in the stator of the bacterial flagellar motor. Biochemistry 40:13041–13050. https://doi.org/10.1021/bi011263o.
16. Nishihara Y, Kitao A. 2015. Gate-controlled proton diffusion and protonation-induced ratchet motion in the stator of the bacterial flagellar motor. Proc Natl Acad Sci U S A 112:7737–7742. https://doi.org/10.1073/pnas.1502991112.
17. Blair DF, Berg HC. 1988. Restoration of torque in defective flagellar motors. Science 242:1678–1681. https://doi.org/10.1126/science.2849208.
18. Leake MC, Chandler JH, Wadhams GH, Bai F, Berry RM, Armitage JP. 2006. Stoichiometry and turnover in single, functioning membrane protein complexes. Nature 443:355–358. https://doi.org/10.1038/nature05135.
19. Lele PP, Hosu BG, Berg HC. 2013. Dynamics of mechanosensing in the bacterial flagellar motor. Proc Natl Acad Sci U S A 110:11839–11844. https://doi.org/10.1073/pnas.1305885110.
20. Liu J, Lin T, Botkin DJ, McCrum E, Winkler H, Norris SJ. 2009. Intact flagellar motor of *Borrelia burgdorferi* revealed by cryo-electron tomography: evidence for stator ring curvature and rotor/C-ring assembly flexion. J Bacteriol 191:5026–5036. https://doi.org/10.1128/JB.00340-09.
21. Beeby M, Ribardo DA, Brennan CA, Ruby EG, Jensen GJ, Hendrixson DR. 2016. Diverse high-torque bacterial flagellar motors assemble wider stator rings using a conserved protein scaffold. Proc Natl Acad Sci U S A 113:E1917–E1926. https://doi.org/10.1073/pnas.1518952113.
22. Tipping MJ, Delalez NJ, Lim R, Berry RM, Armitage JP. 2013. Load-dependent assembly of the bacterial flagellar motor. mBio 4:e00551-13. https://doi.org/10.1128/mBio.00551-13.
23. Chen X, Berg HC. 2000. Torque-speed relationship of the flagellar rotary motor of *Escherichia coli*. Biophys J 78:1036–1041. https://doi.org/10.1016/S0006-3495(00)76662-8.
24. Calvo RA, Kearns DB. 2015. FlgM is secreted by the flagellar export apparatus in *Bacillus subtilis*. J Bacteriol 197:81–91. https://doi.org/10.1128/JB.02324-14.
25. Adler J. 1966. Chemotaxis in bacteria. Science 153:708–716. https://doi.org/10.1126/science.153.3737.708.
26. Armstrong JB, Adler J, Dahl MM. 1967. Nonchemotactic mutants of *Escherichia coli*. J Bacteriol 93:390–398.
27. Julkowska D, Obuchowski M, Holland B, Séror SJ. 2004. Branched swarming patterns on a synthetic medium formed by wild-type *Bacillus subtilis* strain 3610: detection of different cellular morphologies and constellations of cells as the complex architecture develops. Microbiology 150:1839–1849. https://doi.org/10.1099/mic.0.27061-0.
28. Kearns DB, Chu F, Rudner R, Losick R. 2004. Genes governing swarming in *Bacillus subtilis* and evidence for a phase variation mechanism controlling surface motility. Mol Microbiol 52:357–369. https://doi.org/10.1111/j.1365-2958.2004.03996.x.
29. Kearns DB, Losick R. 2005. Cell population heterogeneity during growth of *Bacillus subtilis*. Genes Dev 19:3083–3094. https://doi.org/10.1101/gad.1373905.
30. Calvio C, Celandroni F, Ghelardhi E, Amati G, Salvetti S, Ceciliani F, Galizzi A, Senesi S. 2005. Swarming differentiation and swimming motility in *Bacillus subtilis* are controlled by *swrA*, a newly identified dicistronic operon. J Bacteriol 187:5356–5366. https://doi.org/10.1128/JB.187.15.5356-5366.2005.
31. Guttenplan SB, Shaw S, Kearns DB. 2013. The cell biology of peritrichous flagella in Bacillus subtilis. Mol Microbiol 87:211–229. https://doi.org/10.1111/mmi.12103.
32. Phillips AM, Calvo RA, Kearns DB. 2015. Functional activation of the flagellar type III secretion export apparatus. PLoS Genet 11:e1005443. https://doi.org/10.1371/journal.pgen.1005443.
33. Courtney CR, Cozy LM, Kearns DB. 2012. Molecular characterization of the flagellar hook in *Bacillus subtilis*. J Bacteriol 194:4619–4649. https://doi.org/10.1128/JB.00444-12.
34. DeLange RJ, Chang JY, Shaper JH, Glazer AN. 1976. Amino acid sequence of flagellin of *Bacillus subtilis*. J Biol Chem 251:705–711.
35. LaVallie ER, Stahl ML. 1989. Cloning of the flagellin gene from *Bacillus subtilis* and complementation studies of an in vitro-derived deletion mutation. J Bacteriol 171:3085–3094. https://doi.org/10.1128/jb.171.6.3085-3094.1989.
36. Blair KM, Turner L, Winkelman JT, Berg HC, Kearns DB. 2008. A molecular clutch disables flagella in the *Bacillus subtilis* biofilm. Science 320:1636–1638. https://doi.org/10.1126/science.1157877.
37. Caramori T, Barillà D, Nessi C, Sacchi L, Galizzi A. 1996. Role of FlgM in σ^D-dependent gene expression in *Bacillus subtilis*. J Bacteriol 178:3113–3118. https://doi.org/10.1128/jb.178.11.3113-3118.1996.
38. Fredrick K, Helmann JD. 1996. FlgM is the primary regulator of σ^D activity, and its absence restores motility to a *sinR* mutant. J Bacteriol 178:7010–7013. https://doi.org/10.1128/jb.178.23.7010-7013.1996.
39. Bertero MG, Gonzales B, Tarricone C, Ceciliani F, Galizzi A. 1999. Overproduction and characterization of the *Bacillus subtilis* anti-sigma factor FlgM. J Biol Chem 274:12103–12107. https://doi.org/10.1074/jbc.274.17.12103.
40. Mirel DB, Chamberlin MJ. 1989. The *Bacillus subtilis* flagellin gene (*hag*) is transcribed by the σ^D form of RNA polymerase. J Bacteriol 171:3095–3101. https://doi.org/10.1128/jb.171.6.3095-3101.1989.
41. Mirel DB, Lustre VM, Chamberlin MJ. 1992. An operon of *Bacillus subtilis* motility genes transcribed by the σ^D form of RNA polymerase. J Bacteriol 174:4197–4204. https://doi.org/10.1128/jb.174.13.4197-4204.1992.
42. West JT, Estacio W, Márquez-Magaña L. 2000. Relative roles of the *fla/che* P_A, P_{D-3}, and P_{sigD} promoters in regulating motility and *sigD* expression in *Bacillus subtilis*. J Bacteriol 182:4841–4848. https://doi.org/10.1128/JB.182.17.4841-4848.2000.
43. Hsueh Y-H, Cozy LM, Sham L-T, Calvo RA, Gutu AD, Winkler ME, Kearns DB. 2011. DegU-phosphate activates expression of the anti-sigma factor FlgM in *Bacillus subtilis*. Mol Microbiol 81:1092–1108. https://doi.org/10.1111/j.1365-2958.2011.07755.x.
44. Chen L, Helmann JD. 1994. The *Bacillus subtilis* σ^D-dependent operon encoding the flagellar proteins FliD, FliS, and FliT. J Bacteriol 176:3093–3101. https://doi.org/10.1128/jb.176.11.3093-3101.1994.
45. Mukherjee S, Babitzke P, Kearns DB. 2013. FliW and FliS function independently to control cytoplasmic flagellin levels in *Bacillus subtilis*. J Bacteriol 195:297–306. https://doi.org/10.1128/JB.01654-12.
46. Auvray F, Thomas J, Fraser GM, Hughes C. 2001. Flagellin polymerisation control by a cytosolic export chaperone. J Mol Biol 308:221–229. https://doi.org/10.1006/jmbi.2001.4597.
47. Bange G, Kummerer N, Engel C, Bozkurt G, Wild K, Sinning I. 2010. FlhA provides the adaptor for coordinated delivery of late flagella building blocks to the type III secretion system. Proc Natl Acad Sci U S A 107:11295–11300. https://doi.org/10.1073/pnas.1001383107.
48. Vellanoweth RL, Rabinowitz JC. 1992. The influence of ribosome-binding-site elements on translational efficiency in *Bacillus subtilis* and *Escherichia coli in vivo*. Mol Microbiol 6:1105–1114. https://doi.org/10.1111/j.1365-2958.1992.tb01548.x.
49. Serizawa M, Yamamoto H, Yamaguchi H, Fujita Y, Kobayashi K, Ogasawara N, Sekiguchi J. 2004. Systematic analysis of SigD-regulated genes in *Bacillus subtilis* by DNA microarray and Northern blotting analysis. Gene 329:125–136. https://doi.org/10.1016/j.gene.2003.12.024.
50. Cairns LS, Marlow VL, Bissett E, Ostrowski A, Stanley-Wall NR. 2013. A mechanical signal transmitted by the flagellum controls signalling in *Bacillus subtilis*. Mol Microbiol 90:6–21. https://doi.org/10.1111/mmi.12342.
51. Chan J-M, Guttenplan SB, Kearns DB. 2014. Defects in the flagellar motor increase synthesis of poly-γ-glutamate in *Bacillus subtilis*. J Bacteriol 196:740–753. https://doi.org/10.1128/JB.01217-13.
52. Leibler S, Huse DA. 1993. Porters versus rowers: a unified stochastic model of motor proteins. J Cell Biol 121:1357–1368. https://doi.org/10.1083/jcb.121.6.1357.
53. Ryu WS, Berry RM, Berg HC. 2000. Torque-generating units of the flagellar motor of *Escherichia coli* have a high duty ratio. Nature 403:444–447. https://doi.org/10.1038/35000233.
54. Jenal U, White J, Shapiro L. 1994. *Caulobacter* flagellar function, but not assembly, requires FliL, a non-polarly localized membrane protein present in all cell types. J Mol Biol 243:227–244. https://doi.org/10.1006/jmbi.1994.1650.
55. Schoenhals GJ, Macnab RM. 1999. FliL is a membrane-associated component of the flagellar basal body of *Salmonella*. Microbiology 145:1769–1775. https://doi.org/10.1099/13500872-145-7-1769.

56. Suaste-Olmos F, Domenzain C, Mireles-Rodriguez JC, Poggio S, Osorio A, Dreyfus G, Camarena L. 2010. The flagellar protein FliL is essential for swimming in *Rhodobacter sphaeroides*. J Bacteriol 192:6230–6239. https://doi.org/10.1128/JB.00655-10.
57. Partridge JD, Nieto V, Harshey RM. 2015. A new player at the flagellar motor: FliL controls both motor output and bias. mBio 6:e02367-14. https://doi.org/10.1128/mBio.02367-14.
58. Zhu S, Kumar A, Kojima S, Homma M. 2015. FliL associates with the stator to support torque generation of the sodium-drive polar flagellar motor of *Vibrio*. Mol Microbiol 98:101–100. https://doi.org/10.1111/mmi.13103.
59. Belas R, Suvanasuthi R. 2005. The ability of *Proteus mirabilis* to sense surfaces and regulate virulence gene expression involves FliL, a flagellar basal body protein. J Bacteriol 187:6789–6803. https://doi.org/10.1128/JB.187.19.6789-6803.2005.
60. Attmannspacher U, Scharf BE, Harshey RM. 2008. FliL is essential for swarming: motor rotation in absence of FliL fractures the flagellar rod in swarmer cells of *Salmonella enterica*. Mol Microbiol 68:328–341. https://doi.org/10.1111/j.1365-2958.2008.06170.x.
61. Lee Y-Y, Belas R. 2015. Loss of FliL alters *Proteus mirabilis* surface sensing and temperature-dependent swarming. J Bacteriol 197:159–173. https://doi.org/10.1128/JB.02235-14.
62. Konkol MA, Blair KM, Kearns DB. 2013. Plasmid-encoded ComI inhibits competence in the ancestral 3610 strain of *Bacillus subtilis*. J Bacteriol 195:4085–4093. https://doi.org/10.1128/JB.00696-13.
63. Guérout-Fleury AM, Frandsen N, Stragier P. 1996. Plasmids for ectopic integration in *Bacillus subtilis*. Gene 180:57–61. https://doi.org/10.1016/S0378-1119(96)00404-0.
64. Antoniewski C, Savelli B, Stragier P. 1990. The *spoIIJ* gene, which regulates early developmental steps in *Bacillus subtilis*, belongs to a class of environmentally responsive genes. J Bacteriol 172:86–93. https://doi.org/10.1128/jb.172.1.86-93.1990.
65. Yasbin RE, Young FE. 1974. Transduction in *Bacillus subtilis* by bacteriophage SPP1. J Virol 14:1343–1348.
66. Takahashi Y, Ito M. 2014. Mutational analysis of charged *Bacillus subtilis* residues in the cytoplasmic loops of MotA and MotP in the flagellar motor. J Biochem 156:211–220. https://doi.org/10.1093/jb/mvu030.
67. Ducret A, Quardokus E, Brun YV. 2016. MicrobeJ, a tool for high throughput bacterial cell detection and quantitative analysis. Nat Microbiol 1:16077. https://doi.org/10.1038/nmicrobiol.2016.77.
68. Meister M, Berg HC. 1987. The stall torque of the bacteria flagellar motor. Biophys J 52:413–419. https://doi.org/10.1016/S0006-3495(87)83230-7.